chapter five

REACTION MECHANISMS

5

CONTENTS

SUMMARY

This chapter deals with the application of Density Functional Theory to reaction mechanisms involving metal atoms as a vital and necessary prerequisite. The first part concerns an organic reaction where zinc plays an important role in the aminoalcohol/thiol promoted asymmetric addition of dialkylzincs to aldehydes. In the second part, the mechanism of the reaction taking place in the active site of the copper enzyme quercetinase is studied at all stages of the reaction.

5.1 *Aminothiol/alcohol promoted reactions*

Asymmetric addition of dialkylzincs to aldehydes studied by high-level ab initio calculations

For obvious reasons, the area of catalytic enantioselective synthesis has received an overwhelming amount of interest within organic and inorganic chemistry disciplines. One of the most intriguing and promising observations within this area is the so-called non-linear effect (or chiral amplification); i.e. the achievement of an enantiomeric excess (e.e.) of a product exceeding the e.e. of the catalyst used. For instance, exploitation of this effect obviates the need to obtain catalysts with a very high e.e., which usually is a very costly exercise.

One of the most impressive examples of non-linearity in catalytic enantioselective synthesis has been found in the (2S)-3-exo-(dimethylamino)isobornenol (DAIB) catalyzed methylation of benzaldehyde by dimethylzinc (Figure 5.1.1), as studied by Noyori and co-workers[238-244]. It has been demonstrated that this particular reaction exhibits an extremely large non-linear effect; e.e.'s of over 90 % have been achieved for the formed (S)-1-phenylethanol using DAIB in an e.e. of just 20 %.

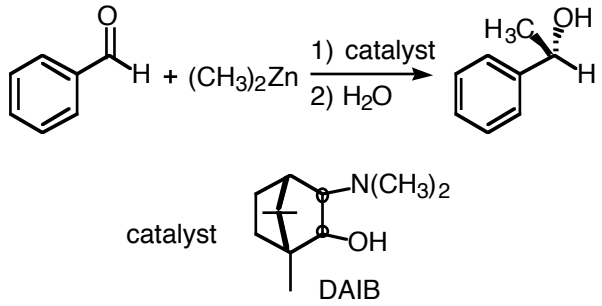

FIGURE 5.1.1. ASYMMETRIC ADDITION OF DIMETHYLZINC TO BENZALDEHYDE CATALYZED BY (DIMETHYLAMINO)ISOBORNENOL

Noyori et al. have studied this reaction in great detail[238-244], both experimentally and theoretically, with the aim to provide more insight into the origin of the non-linear effect. A remarkable and highly relevant experimental observation has been the dramatic decrease in reaction rate when using non-racemic mixtures of both stereoisomers of DAIB instead of using the enantiomerically pure compound as catalyst. This unambiguously indicates that the presence of both stereoisomers causes a partial inhibition of the catalytic cycle. To provide an explanation these findings, an attempt has been made to identify the various intermediate structures of the catalytic cycle by means of quantumchemical calculations at the MP2 level of theory using 2-aminoethanol as model ligand. These efforts have resulted in a proposed catalytic cycle as depicted in Figure 5.1.2.

In this cycle, the methylzinc aminoalkoxide **1** is proposed to be the catalytically active species. Subsequently, an aldehyde and another dimethylzinc moiety are coordinated to methylzinc aminoalkoxide **1** leading to active species **5** via species **3** or **4**, from which the alkylation of the aldehyde takes place. The conformation of **5** is held responsible for the obtained enantioselectivity; on the basis of the aforementioned model calculations. This

view has been corroborated by additional MP2 calculations using DAIB as ligand; both calculations demonstrated that an anti-configuration of the involved transition state is the more stable conformation, thus rationalizing the predominant formation of (S)-1-phenylethanol.

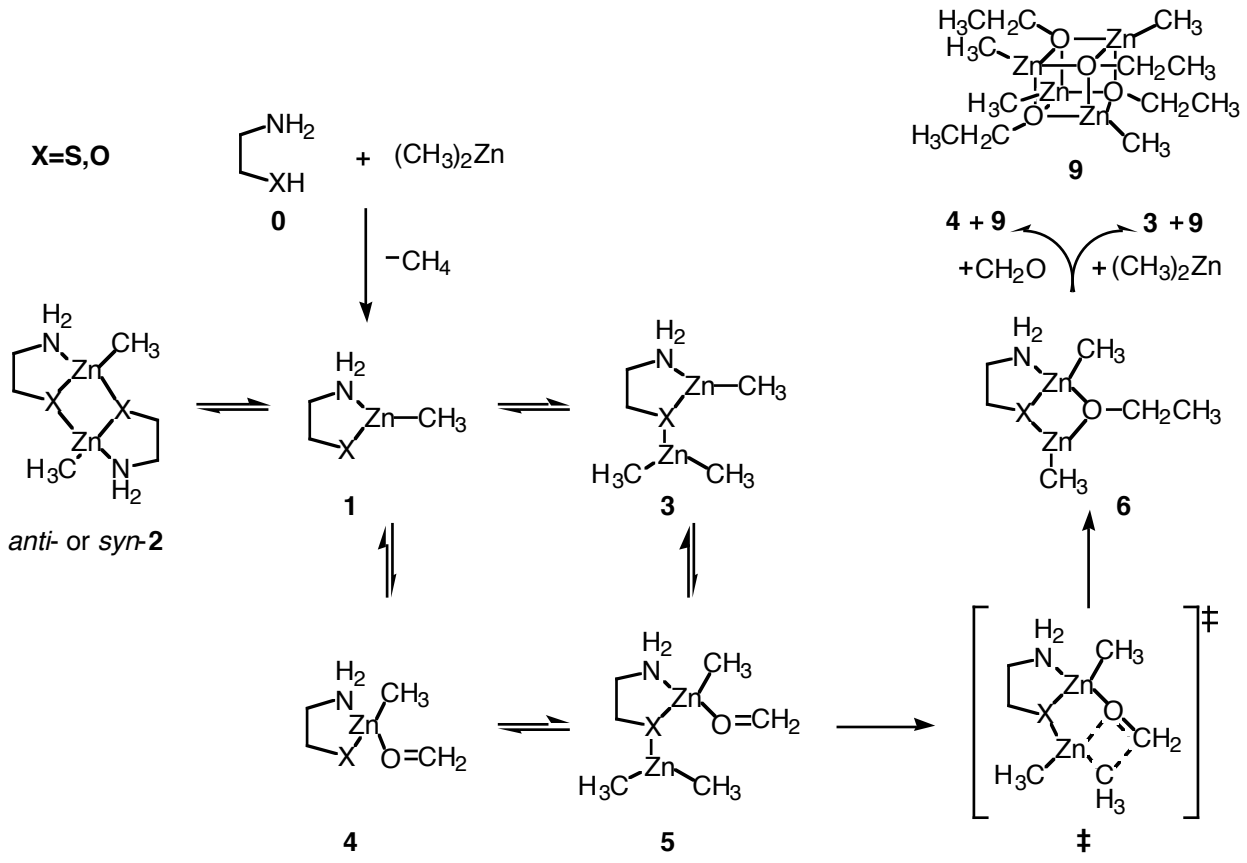

FIGURE 5.1.2. PROPOSED REACTION MECHANISM USED IN MP2 STUDY OF MODEL SYSTEM[243]

The MP2 model study also confirmed that methylzinc aminoalkoxide **1** is capable of dimerizing to methylzinc aminoalkoxide dimer **2**. Dimer **2** appeared to exhibit two minimal energy conformations; a syn-conformation in which the two methyl groups of the zinc are oriented on the same side of the central Zn-O-Zn-O ring, and an anti-conformation in which these methyl groups are oriented on opposite sides of the central four-membered ring. The MP2 calculations revealed that the anti-conformation of **2** was the more stable of the two by approximately 3 kcal/mole. In addition, the dimers **2** were calculated to be over 35 kcal/mole more stable than two non-interacting monomers **1**, a much larger stabilization in comparison with the other intermediate structures in the catalytic cycle.

The formation of the methylzinc aminoalkoxide dimers **2** has been linked to the occurrence of the non-linear effect of chiral amplification in the DAIB catalyzed alkylation of benzaldehyde. It has been expected that, in the case of chiral monomers **1**, e.g. DAIB, the meso (R,S)-dimer **2** will adopt the anti-conformation, as opposed to the optically active (R,R)- or (S,S)-dimers **2**, which will adopt the syn-conformation. Since the anti-conformer is expected to be the more stable conformer on the basis of the aforementioned MP2 calculations, not only can it be expected that the meso-dimer **2** is predominantly formed, but the release of the (R)- and (S)-monomers **1** from meso dimer **2** is also (much) slower than the

release of the monomers **1** from the optically active syn-dimers **2**. This results in an enhancement of e.e. of free monomer **1** in solution, although the concentration of free monomer **1** is reduced, because a significant amount of monomer **1** is captured in the very stable dimer form **2**, resulting in a negative effect on the reaction rate. Consequently, this mechanistic model provides a highly plausible explanation for both the chiral amplification as well as for the reduction in reaction rate in the case of non-racemic mixtures of DAIB.

Recently, a mathematical study[245] in which experimentally available data has been fitted to appropriate formulas has confirmed the validity of this picture. In addition, it has provided valuable insights into the requirements for the occurrence of chiral amplification in such reactions; it has been suggested that, apart from the required energetic discrimination between the meso- and optically active forms of the aggregates, the release of catalytically active monomer from their aggregated structures should be slow in comparison to the reaction rate of the catalytic process, in order to obtain a substantial chiral amplification in the catalysis. If such release would be fast in comparison to the rate of the catalytic process, both meso and optically active aggregates would be capable of substantial dissociation on the time scales of the catalytic cycle, which would have a detrimental effect on the desired non-linear effect due to the release of both stereoisomers of the catalyst.

The striking success of the DAIB catalyzed alkylation of benzaldehyde has sparked a large number of experimental investigations in an attempt to emulate the results achieved by Noyori et al. One of the more interesting results from these efforts have been presented by Kellogg et al. (see Figure 5.1.3)[246-250].

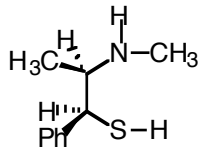

H1

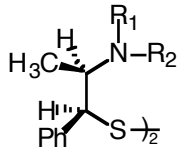

H3

	R_1	R_2
a	H	CH_3
b	CH_3	CH_3
c	CH_3	$CH(CH_3)_2$

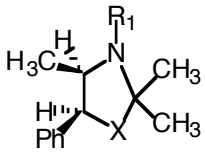

H4

	R_1	X
a	CH_3	S
b	H	S
c	CH_3	O
d	H	O

FIGURE 5.1.3. CORRESPONDING AMINOTHIOL CATALYSTS STUDIED BY KELLOGG ET AL.

They demonstrated that the replacement of aminoalcohols by corresponding aminothiol or aminothiol derivatives generally resulted in an increase of the enantiomeric excess of the formed secondary alcohols as well as in an increase of the rate of the reaction. In addition, they proposed a catalytically active species similar to the species proposed by Noyori et al. in

their work. This has led to the assumption that replacement of the oxygen by a sulfur atom in the catalytically active complex improves the catalytic properties of the ligand, an assumption that has been confirmed by subsequent investigations[251-255]. In these investigations, it was shown that the replacement of the oxygen by sulphur increases also the chiral amplification.

This raises an interesting question: why do the aminothiol (derivatives) appear to induce higher enatioselectivity in the formation of optically active secondary alcohols, higher reaction rates as well as a larger chiral amplification ? The work presented in this study aimed at finding an answer to this intriguing question. To obtain this answer, high-level *ab initio* studies have been performed at the Density Functional Theory[1] and MP2 level of theory in which the catalytic cycles associated with the 2-aminoethanethiol and 2-aminoethanol promoted methylation of formaldehyde by dimethylzinc have been compared. In these studies, basis sets of triple zeta quality have been used, and a full counterpoise correction of the BSSE has been included for all single-point energy calculations in order to achieve both qualitatively and quantitatively reliable results. It will be demonstrated that, especially at the MP2 level of theory, large basis set superposition errors can occur, which, if left unaccounted for, can lead to serious misinterpretations of the relative energies associated with the various intermediate minimal energy structures.

Computational details

In this study, the same model reaction as investigated by Yamakawa and Noyori[243] has been used, i.e. the reaction of dimethylzinc and formaldehyde promoted by either 2-aminoethanol or 2-aminoethanethiol (see Figure 5.1.2). As the formation of the cage compound **9** after the formation of compound **6** seems to be favorable and not involved in either the reaction rate or the enantioselectivity, this step in the reaction has been ignored in this study. For each conformation along the reaction path, a full geometry optimization was performed using Density Functional Theory (DFT) calculations[1] with the Becke[120]-Perdew[121] exchange-correlation potential in a triple zeta valence with polarization functions (TZP) basis set of Slater type orbitals.

The geometries of the molecules were obtained using the ADF program[117,187] with the DIIS scheme and the BFGS scheme for updating the Hessian. For the transition state (TS) the Powell update scheme was used, since this is more appropriate for a non-equilibrium geometry optimization. The DFT- calculations were carried out with the ADF program[117,187] on a Linux-cluster of Pentium-nodes as well as on a cluster of IBM/RS6000 workstations. The structures were refined until the gradient was below a threshold of 1.0e-3 a.u. The validity of the obtained structures was checked by inspecting the eigenvalues of the Hessians of these structures, which all proved to exhibit zero negative eigenvalues for the equilibrium structures and one *and only one* for the transition structures, as required by the transition state theory.

The starting structure for locating the transition state was obtained with the SADDLE approach in MOPAC93[219], using the AM1 Hamiltonian. This Hamiltonian, although a bit less accurate than the PM3 option, normally provides transition structures which are very close to those obtained with more robust methods when used in conjunction with the SADDLE approach. Subsequent optimization with *ab initio* methods normally converges rapidly, as

has been the case for our investigations as well. In the here presented studies, we used Cartesian coordinates in MOPAC, but Z-matrix coordinates in the ADF program, in order to be able to use an approximate Hessian in the TS localization. With this choice of coordinates, we were able to explicitly use internal coordinates involved in the transition, which we took for instance to be the two bonds that are broken (Zn-CH3) and formed (CH2-CH3) in the process of going from conformation **5** to **6**. The diagonal element in the Hessian for these two coordinates was given an initial negative value, while the rest of the Hessian was filled using the normal procedure. This scheme proved to converge rapidly.

Using the optimized structures, the interaction energy could be obtained as follows (with $U^{full}(1..N_m)$ the total energy of the system, N_m the total number of monomers and $U^{i,eq}(i)$ the energy of monomer i in its equilibrium geometry):

$$\Delta U_{simple} = U^{full}(1..N_m) - \sum_{i}^{N_m} U^{i,eq}(i) \tag{1}$$

However, this is valid only when using a basis set with an infinite number of functions, or at least a sufficient number to reach the basis set limit. This limit is normally reached only with extensively large basis sets. For smaller basis sets, we can still obtain reasonable interaction energies, after correcting the results for the Basis Set Superposition Error (BSSE) using the full counterpoise method[1]. The BSSE-corrected energy profile is then obtained as:

$$\Delta U_{interaction} = U^{full}(1..N_m) - \sum_{i}^{N_m} \left(U^{full}(i) - U^{i,cmplx}(i) + U^{i,eq}(i) \right) \tag{2}$$

Here, $U^{full}(1...N_m)$ is the total energy of the complex in the complete basis (i.e. of all N_m monomers), $U^{full}(i)$ the energy of monomer i in the complete basis at the complex geometry, $U^{i,cmplx}(i)$ the energy of monomer i in the monomer basis at the complex geometry and $U^{i,eq}(i)$ the energy of monomer i in the monomer basis at its equilibrium geometry. In the following, we will refer to the BSSE correction energies as follows:

$$\Delta U_{correction} = \sum_{i}^{N_m} \left(U^{i,cmplx}(i) - U^{full}(i) \right) \tag{3}$$

The corrected energies ($\Delta U_{interaction}$) are then obtained by taking the sum of ΔU_{simple} and $\Delta U_{correction}$.

The computed Hessians for the structures were used also to obtain thermodynamic properties like the enthalpy H_{rvt}, entropy S_{rvt} and Gibbs free energy G_{rvt} from the rotations, vibrations and translations of the molecules. Once the vibrational frequencies are known, it is straightforward[1,256] to calculate these properties (see Appendix 5.1). The obtained Gibbs free energies G_{rvt} should then be added to the DFT energies to obtain the total Gibbs energies G_{tot}.

The obtained optimized structures were used also to obtain the full counterpoise BSSE-corrected energy profile with single point restricted second-order Møller-Plesset perturbation (MP2) calculations in a 6-311G** basis set for all atoms. All electrons were included in the correlation. These calculations were carried out using the HONDO program[204,225] on a Linux-cluster of Pentium-nodes.

Results and discussion

Summary

The asymmetric addition of dialkylzincs to aldehydes promoted by aminoalcohol or aminothiol has been carefully investigated by high level *ab initio* calculations. The geometries of all relevant conformations in the proposed reaction mechanism (see Figure 5.1.2) were optimized using Density Functional Theory calculations. The energies obtained for these conformations were corrected for Basis Set Superposition Errors, and thermodynamic properties (enthalpy, entropy and Gibbs free energy) obtained from the computed Hessians. These Hessians resulted in zero negative eigenvalues for equilibrium structures and one *and only one* negative eigenvalue for transition structures.

Energies

The energies obtained from the DFT calculations are given in Table 5.1.1. Reported in this Table are the total and the BSSE correction energies, as well as the thermodynamic properties at 298.15 K. For the conformations **6** and **5**-TS no BSSE corrections are needed, as they are obtained with the same number of basis functions as conformation **5**; therefore, the energies can be compared directly. The relative energies resulting from these energies, corrected for BSSE, are given in Table 5.1.2, together with the relative Gibbs free energies G_{rvt} and G_{tot}. The MP2 energies are reasonably similar to the DFT energies (deviations of a few kcal/mol), with a few exceptions. The BSSE corrections are in all cases many times larger than those found in the DFT calculations; in all cases of the same magnitude as the *corrected* interaction energy itself. For instance for the *anti*-**2** (sulphur) conformation, ΔU_{simple} is −18.30 kcal/mol, $\Delta U_{correction}$ 15.94 kcal/mol and therefore the corrected energy $\Delta U_{interaction}$ only −2.37 kcal/mol. The BSSE corrections can therefore play a very significant role and can not be safely ignored if MP2 calculations are used. For the DFT calculations on the other hand, they are much smaller (due to the use of Slater type orbitals) and meaningful interpretations can be obtained also without taking the BSSE corrections explicitly into account.

Structures

Some structural parameters for the geometries of the conformations are given in Table 5.1.3. Some differences between the aminoalcohol and aminothiol geometries are observed (mainly for *Zn-X* distances), but on the whole a large similarity between them is found. On average, the *Zn-S* distances are some 0.4 Å larger than the *Zn-O* distances.

Dimerization

The dimerization of **1** into either an anti- or syn-complex **2** is in all cases favorable by some 10-22 kcal/mol when looking at the DFT energy only. However, the Gibbs free energies are found at much lower values (from −5.8 to +2.2 kcal/mol) and, interestingly enough, are much closer to the experimentally observed ones[254] that were estimated as −2.1 kcal/mol for the thiol and −4.6 for the alcohol. Although the actual aminoalcohol and aminothiol in these studies are different (which may explain the observed differences), the good agreement between experiment and theory may give a clue about the calculated results.

For both the aminoalcohol and aminothiol dimers **2**, the *syn*-conformation is less stable than the *anti*-conformation by some 6 kcal/mol in terms of the DFT energy. For the aminothiol dimers, almost the same energy difference is observed in terms of the Gibbs free energy. The *anti*-conformation of the aminoalcohol dimer **2** however is destabilized with respect to the *syn*-conformation by the entropy contribution to the free energy, leading to a smaller difference in terms of the Gibbs free energy of only 3.5 kcal/mol. This can have a marked effect on the relative stabilities of the optically active (R,R) or (S,S) *syn*-dimers with respect to the meso (R,S) *anti*-dimer, and could explain the higher e.e.'s observed in thiols vs. alcohols.

TABLE 5.1.1. DFT ENERGIES AND THERMODYNAMIC PROPERTIES (AT 298K)

	DFT energy		H_{rvt}	S_{rvt}	G_{rvt}
	Hartree	*Hartree*	*kcal/mol*	*cal/mol/K*	*kcal/mol*
diMeZn	-1.4566		46.50	71.05	25.32
formaldehyde	-0.8051		18.41	53.68	2.41
X=S	*full*	*BSSE*			
1	-2.6564		80.47	96.02	51.84
anti-2	-5.3410	0.0020	162.05	152.74	116.51
syn-2	-5.3317	0.0018	161.77	151.55	116.59
3	-4.1158	0.0007	127.59	129.93	88.85
4	-3.4649	0.0007	99.63	115.70	65.13
anti-5	-4.9260	0.0017	147.39	154.31	101.38
syn-5	-4.9250	0.0017	146.76	149.82	102.09
anti-5-TS	-4.9237		148.50	145.19	105.21
syn-5-TS	-4.9133		147.13	137.57	106.12
6	-4.9958		149.91	139.54	108.30
X=O					
1	-2.7436		81.18	94.27	53.07
anti-2	-5.5254	0.0025	162.55	133.72	122.68
syn-2	-5.5152	0.0023	163.28	145.45	119.91
3	-4.2090	0.0011	128.96	132.43	89.48
4	-3.5543	0.0008	100.98	114.00	66.99
anti-5	-5.0190	0.0021	147.61	142.76	105.05
syn-5	-5.0175	0.0020	149.33	159.84	101.67
trans-5	-5.0203	0.0020	148.80	152.88	103.22
anti-5-TS	-5.0135		148.17	130.49	109.26
syn-5-TS	-5.0062		147.96	131.19	108.84
6	-5.0884		151.45	141.34	109.30

In an attempt to get a reliable comparison for the effectiveness of either aminoalcohol or aminothiol compounds, Kang et al.[255] investigated the catalytic activity of either the pure thiol, or the pure corresponding alcohol, or a 1:1 mixture of the two. It was found that the thiol is approximately eight times more effective than the alcohol. In order to check whether some unexpected results would occur for the *syn*- or *anti*-conformations of such mixed dimers, the same procedure as for the *pure* compounds were followed; i.e. the geometries optimized, energies calculated and corrected for BSSE and thermodynamic properties

obtained from the computed Hessians. The Gibbs free energies for the *anti*- and *syn*-conformations were found to be –4.48 and –0.46 kcal/mol respectively. These numbers are almost equal to the average of the aminoalcohol and aminothiol values for the *anti*- (–4.72 kcal/mol) or *syn*-conformations (-0.09 kcal/mol).

TABLE 5.1.2. RELATIVE ENERGIES (KCAL/MOL) OF CONFORMATIONS

	DFT energy		ΔG_{rvt}	ΔG_{total}
X=S	*full*	*BSSE*		
1	0.00		0.00	0.00
anti-**2**	-16.43	*1.26*	12.83	-3.60
syn-**2**	-10.72	*1.10*	12.91	2.19
3	-3.00	*0.41*	11.69	8.69
4	-2.45	*0.44*	10.88	8.43
anti-**5**	-6.33	*1.08*	21.81	15.48
syn-**5**	-5.64	*1.08*	22.52	16.88
anti-**5**-TS	-4.86		25.64	20.78
syn-**5**-TS	1.69		26.55	28.24
6	-50.12		28.74	-21.38
X=O				
1	0.00		0.00	0.00
anti-**2**	-22.39	*1.57*	16.55	-5.84
syn-**2**	-16.13	*1.47*	13.77	-2.36
3	-6.58	*0.66*	11.09	4.51
4	-3.77	*0.51*	11.51	7.74
anti-**5**	-9.76	*1.29*	24.25	14.49
syn-**5**	-8.83	*1.28*	20.88	12.05
trans-**5**	-10.60	*1.24*	22.43	11.83
anti-**5**-TS	-6.28		28.47	22.19
syn-**5**-TS	-1.74		28.05	26.31
6	-53.37		28.51	-24.86

Complexation of dimethylzinc

The complexation of dimethylzinc to the aminoalcohol/thiol is accompanied by a change of the angle between the two methylgroups in dimethylzinc. While its equilibrium structure is linear, upon complexation the angle decreases to 160° (alcohol) or 165° (thiol conformation). This enables a closer approach to the Zn-complex at either 2.27 (alcohol) or 2.92 Å (thiol), and is accompanied by a favorable DFT energy of –6.6 (alcohol) and –3.0 kcal/mol (thiol). The Gibbs free energy on the other hand is less favorable than conformation **1** by some 4.5 (alcohol) and 8.7 kcal/mol (thiol). If the Zn-complex **1** is visualized as a plane with oxygen/sulphur on the left and nitrogen on the right hand side, dimethylzinc is being found below this plane.

Complexation of formaldehyde

Upon complexation of formaldehyde with conformation **1** to form **4**, a remarkable result is obtained. For the aminoalcohol structure, the formaldehyde molecule is found above the plane of the Zn-complex, while for the aminothiol structure it is found below the plane, like

observed for dimethylzinc. To check whether this may have been influenced by the starting structures for the optimizations, the oxygen and sulphur atoms were switched and the geometries reoptimized; this lead to the same structures that had already been found. The complexation leading to **4** is accompanied by a decrease in DFT energy of –3.8 (alcohol) and –2.5 kcal/mol (thiol), and an increase in Gibbs free energy of 7.7 (alcohol) and 8.4 kcal/mol (thiol).

TABLE 5.1.3. SOME RELEVANT STRUCTURAL PARAMETERS (BONDS IN Å)

compound	*X=S*	*X=O*	*compound*	*X=S*	*X=O*
1					
Zn1-X	2.256	1.870	*Zn1-NH₂*	2.300	2.324
anti-**2**			*syn*-**2**		
Zn1-X1	2.476	2.087	*Zn1-X1*	2.469	2.087
Zn1-NH₂	2.243	2.240	*Zn1-NH₂*	2.277	2.312
Zn1-X2	2.483	2.052	*Zn1-X2*	2.523	2.059
3			**4**		
Zn1-X	2.274	1.902	*Zn1-X*	2.288	1.910[a]
Zn1-NH₂	2.287	2.311	*Zn1-NH₂*	2.260	2.267[a]
Zn3-X	2.921	2.269	*Zn1-O*	2.848	2.719[a]
anti-**5**			*syn*-**5**		
Zn1-X	2.316	1.943	*Zn1-X*	2.316	1.944
Zn1-NH₂	2.237	2.239	*Zn1-NH₂*	2.247	2.254
Zn1-O	2.568	2.524	*Zn1-O*	2.631	2.563
Zn3-X	2.756	2.214	*Zn3-X*	2.769	2.267
Zn3-Me	1.994	2.004	*Zn3-Me*	1.998	2.011
Me-CH₂	4.156	3.939	*Me-CH₂*	4.200	4.026
anti-**5**-TS			*syn*-**5**-TS		
Zn1-X	2.433	2.056	*Zn1-X*	2.427	2.032
Zn1-NH₂	2.226	2.220	*Zn1-NH₂*	2.255	2.284
Zn1-O	2.142	2.139	*Zn1-O*	2.156	2.158
Zn3-X	2.416	2.033	*Zn3-X*	2.426	2.039
Zn3-O	2.532	2.561	*Zn3-O*	2.493	2.471
Zn3-Me	2.179	2.164	*Zn3-Me*	2.220	2.196
Me-CH₂	2.269	2.266	*Me-CH₂*	2.280	2.331
6					
Zn1-X	2.471	2.088	*Zn3-X*	2.432	2.020
Zn1-NH₂	2.287	2.298	*Zn3-O*	1.979	1.967
Zn1-O	2.059	2.041	*O-CH₂*	1.429	1.427

a) Found as *trans*

*Active species **5***

The complexation of both dimethylzinc and formaldehyde may occur in a few different orientations: the formaldehyde may be oriented either *syn* or *anti* with respect to the methyl group connected to the zinc atom of **1**. For the aminoalcohol even a third orientation (*trans*) is observed, where the formaldehyde is located above the plane of **1**, while the dimethylzinc is found a bit below this plane. As the distance between either one of the methyl groups and the CH_2 group of formaldehyde are so far apart, this *trans* orientation is not significantly involved in the reaction leading to conformation **6**. Apart from energetic considerations the

influence of the *syn*/*anti* orientation may be safely ignored for formaldehyde; however for larger aldehydes like the ones used in the actual experiments (benzaldehyde), this *syn*/*anti* orientation determines the enantiomericity of the product. In either the *syn*- or *anti*-conformation, the formaldehyde is already favorably oriented towards either one of the methyl groups of dimethylzinc. For both aminoalcohol and aminothiol, the *anti*-conformation is found to be more stable than the *syn*-conformation in terms of the DFT energy. In terms of the Gibbs free energy this holds also for the aminothiol, but not for the aminoalcohol, which is in both cases to a large extent resulting from entropy contributions. In the transition structures leading from **5** to **6** formaldehyde has moved towards the zinc of **1** by some 0.4-0.5 Å, while also the forming bond between the methyl and CH_2 groups is decreased to a large extent to some 2.27-2.33 Å. At the same time, the distance of the moving methyl group from zinc has increased from 1.99-2.01 to 2.16-2.22 Å, while the C-O distance in formaldehyde increased to 1.28 Å. The transition states are for both the aminoalcohol and aminothiol favorable in the *anti*-orientation by either 4.1 (alcohol) or 7.5 (thiol) kcal/mol. The Gibbs free energy of the transition state is 1.4 kcal/mol lower for the aminothiol promoted reaction than for the aminoalcohol.

Formation of the "product"

The formation of conformation **6** is exothermic after **5** or **5**-TS by almost 21-25 kcal/mol relative to **1**. Compared to the most stable structure of **5**, it is even ~36 kcal/mol more stable. The distance of the formaldehyde oxygen to both zinc atoms is decreased considerably; for both the alcohol and the thiol, the distance towards the zinc of **1** is ~2.05 Å, while it is even closer to the zinc of dimethylzinc at ~1.97 Å. The subsequent steps in the reaction, leading eventually to the product **9** do not involve discriminating features for either reaction rate or enantiomeric excess, and are therefore not investigated.

Conclusions

The aminoalcohol and aminothiol promoted conversion of aldehydes into secondary alcohols by dialkylzinc has been investigated by high-level *ab initio* calculations using 2-aminoethanethiol and 2-aminoethanol as model ligands with dimethylzinc and formaldehyde as reactants. The associated catalytic cycles have been investigated using Basis Set Superposition Error (BSSE) corrected Density Functional Theory (DFT) in a TZP basis set as well as by BSSE corrected MP2/6-311G** calculations. It has been demonstrated that, unlike the DFT method, the MP2 method introduces large BSSE effects in interaction energies of interest, emphasizing the need for the explicit inclusion of BSSE corrections at this level of theory when trying to establish quantitatively accurate estimates of such energies. Finally, it has been demonstrated that the catalytic cycles of the aminoalcohol and aminothiol promoted reactions are quite similar, although the local minima of the intermediate structures of interest on the potential energy surface of the aminothiol promoted reaction are more shallow in comparison to those of the aminoalcohol promoted reaction. This observation is used to provide a rational model in terms of thermodynamic equilibria explaining the enhanced kinetics and chiral amplification in the aminothiol promoted reactions.

Appendix 5.1. Computation[a] of thermodynamical properties[1,256]

Enthalpy H

$$H(T) = H_{translation}(T) + H_{rotation}(T) + \Delta H_{vibrational}(T) + RT$$

$$\begin{aligned} H_{translation}(T) &= \tfrac{3}{2}RT \\ H_{rotation}(T) &= \tfrac{3}{2}RT \quad (RT \text{ for linear molecule}) \\ \Delta H_{vibrational}(T) &= H_{vibrational}(T) - H_{vibrational}(0) \\ \Delta H_{vibrational}(T) &= Nh \sum_{i}^{normal\ modes} \frac{\nu_i}{\left(e^{h\nu_i/kT} - 1\right)} \\ \Delta H_{vibrational}(0) &= E_{zero\text{-}point} = \tfrac{1}{2}h \sum_{i}^{normal\ modes} \nu_i \end{aligned} \tag{4}$$

Entropy S

$$S = S_{translation} + S_{rotation} + S_{vibration} + S_{electronic} - nR\left[\ln\left(nN_{av}\right) - 1\right]$$

$$\begin{aligned} S_{translation} &= nR\left[\tfrac{3}{2} + \ln\left[\left(\frac{2\pi MkT}{h^2}\right)^{3/2}\left(\frac{nRT}{p}\right)\right]\right] \\ S_{rotation} &= nR\left[\tfrac{3}{2} + \ln\left[\frac{\sqrt{\pi u_a u_b u_c}}{s}\right]^{1/2}\right] \\ S_{vibration} &= nR\sum_{i}\left\{\left(\Theta_i e^{\Theta_i} - 1\right)^{-1} - \ln\left(1 - e^{-\Theta_i}\right)\right\} \\ S_{electronic} &= nR\ln w_{electronic} \end{aligned} \tag{5}$$

In these formulas, the following parameters are used:

n	moles of molecules
R	gas constant
N_{av}	Avogadro's constant
M	mass of molecule
k	Boltzmann's constant
T	temperature
h	Planck's constant
p	pressure
I_a, I_b, I_c	principal moments of inertia
u_a,u_b,u_c	$h^2/8\pi I_a kT$, .. , ..
s	symmetry number
ν_i	vibrational frequencies
Θ_i	$h\nu_i/kT$
w_{el}	electronic ground state degeneracy

[a] Formulas given in SI units

5.2 *Quercetinase*

A density functional theory investigation of the reaction mechanism of Aspergillus japonicus Quercetinase[a]

Oxygenases are a class of enzymes that catalyze the incorporation of oxygen atoms from dioxygen into a substrate. They can be divided into two subclasses depending on whether both atoms of dioxygen are incorporated in the substrate (*dioxygenases*) or only one of them (*monooxygenases*). In almost all cases are dioxygenases iron metalloenzymes. Quercetinase (also known as quercetin 2,3-dioxygenase or flavonol 2,4-dioxygenase) is one of a few examples where instead a copper atom is involved[257,258]. This enzyme facilitates the incorporation of dioxygen into quercetin, thereby cleaving its heterocyclic ring to produce the corresponding depside (phenolic carboxylic acid ester) and carbon monoxide (see Figure 5.2.1).

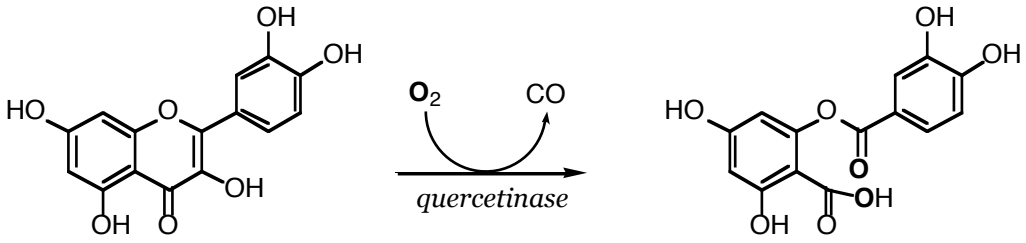

FIGURE 5.2.1. PROCESS CATALYZED BY QUERCETINASE

The crystal structure from *Aspergillus japonicus* has recently been solved[259]. The native structure shows an active site with a copper atom coordinated by three histidine residues (His66, His68, His112) at 2.09-2.16 Å and a water molecule at 2.21 Å (*major* conformation); an additional coordination is present, in which a glutamate residue (Glu73) is coordinated at 2.10 Å, while the water molecule is found at a larger distance of 2.41 Å (*minor* conformation). The co-existence of these two conformations is also present in the native EPR spectrum[260], which presents a mixed signal.

Upon binding of the substrates kaempferol or quercetin (KMP and QUE, see Figure 5.2.2)[261,262], a flexible loop (residues 155-169) shields the active site from solvent molecules. The substrate replaces the water molecule as copper ligand, while the glutamate fully coordinates at a distance of 1.97 Å (KMP) in the crystal structure[261,262]. A close interaction between the $O_{\square 2}$ atom of Glu73 and the O_3 atom of the substrate (2.43 Å in KMP) suggests a role for the glutamate residue in the deprotonation of the 3OH group (see Figure 5.2.2 for atom numbering). Deprotonation is likely to occur in order for a proper binding of the substrate to the copper to be established. Although the proton may be exchanged with either solvent or the protein environment, a 1000-fold decrease in activity for the Glu73Gln mutant and the proper positioning of the glutamate residue seems to suggest a role for this residue in the deprotonation[261]. Keeping the proton in close approximity could also be advantageous for protonating the depside product prior to its release.

---

[a] Joint study by R.A. Steiner and M. Swart, who contributed equally to this work.

Another intriguing feature observed in the crystal structure is that the substrates are no longer flat; the C-ring (see Figure 5.2.2 for its definition) is bent out of the plane defined by the rest of the molecule by about 10°. This bending might be the result of steric interactions with the nearby Phe75 and Phe114 residue side chains.

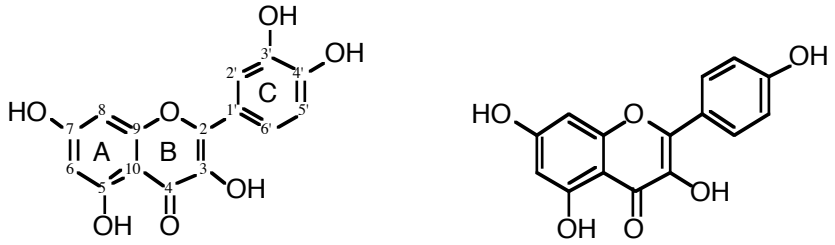

quercetin *kaempferol*

FIGURE 5.2.2. SUBSTRATES INVOLVED WITH QUERCETINASE

A possible reaction mechanism for the quercetinase-mediated dioxygenation of flavonols is shown in Figure 5.2.3. Upon binding of the substrate, accompanied by the closure of the active site through the flexible loop, the Glu73 residue abstracts the proton from the 3OH group of the substrate, to form **2**. A tautomer of this conformation is also possible (**2taut**) where part of the unpaired electron of the copper atom is transferred to carbon 2 giving rise to some radical character on this atom. In the following step, the binding of dioxygen occurs, which can lead to two different routes; in route **a** the (diradical) dioxygen binds to C2 to form the peroxide **3a**, which would lead to the endoperoxide **4** after nucleophilic attack on C4. In the alternative route **b**, the dioxygen binds first to copper (**3b**), a radical combination step occurs (**3b2**) and through a nucleophilic attack, the same endoperoxide **4** is formed. In the next step, the endoperoxide is transformed into the depside **5**, which is accompanied by the leaving of carbonmonoxide. Finally, the depside is protonated (possibly abstracting its proton from the Glu73 residue) and leaves the active site, which is ready for a next cycle.

Route **a** in this proposed reaction mechanism is supported by the crystal structures of quercetinase complexed with QUE and KMP, in which the C2 atom is found pyramidalized. This geometry indicates the possibility of a stabilization of the radical species on C2. The reactive complex arises from an intramolecular radical transfer from the predominant flavonol-Cu(II) species **2**. It is expected to have a low steady-state concentration and to be not easily detectable spectroscopically. To date, EPR evidence for such a species has not been obtained in protic media and only once in the oxygenation reaction of potassium flavonolate to *O*-benzoylsalycilate in DMF[263]. Of similar difficulty appears to be the trapping of endoperoxide **4**, which has not yet been characterized or isolated[263].

In order to obtain insights on the possible reaction intermediates involved in the enzymatic process catalyzed by quercetinase, a Density Functional Theory[1] (DFT) investigation was performed using the experimentally determined copper coordination in the active site. Starting from the crystal structure of quercetinase with the fastest[261] substrate KMP, both routes **a** and **b** have been analyzed as possibilities for dioxygen attack.

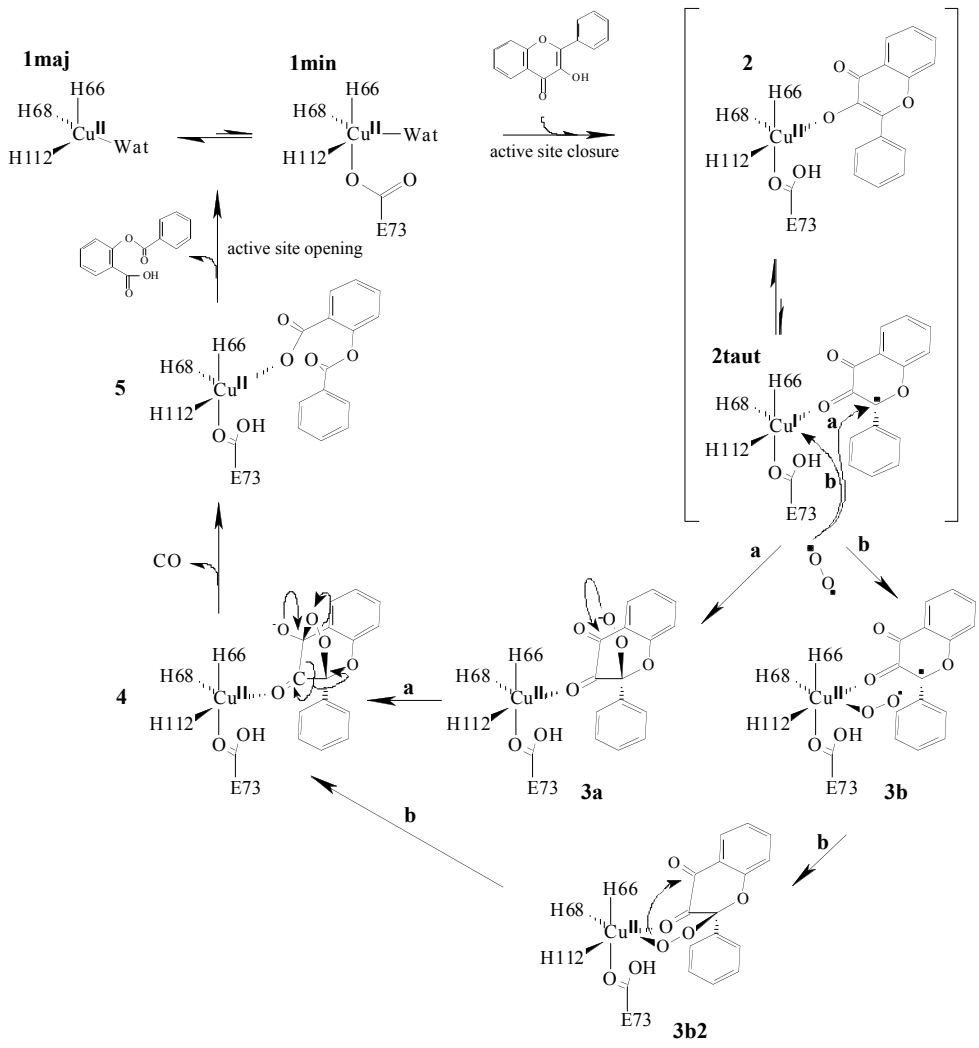

FIGURE 5.2.3. PROPOSED REACTION MECHANISM FOR QUERCETINASE

Computational details

A mechanistic study of the quercetinase-catalyzed dioxygenation of the flavonol kaempferol was carried out using Density Functional Theory[1] (DFT) calculations with the ADF[117,187] program (version 2000.01) using the Becke[120]-Perdew[121] exchange-correlation potential in a triple zeta valence with polarization functions basis set (TZP) of Slater type orbitals. In addition to the copper ion, and other relevant molecules depending on the reaction step under consideration, the proteic copper-ligands (His66, His68, Glu73 and His112), truncated at the Cα atom, were included; on average, this amounted to about 90 atoms. Hydrogens were added where appropriate, resulting in a methyl group at the Cα position. Each structure was subjected to a full geometry optimization, in which the structures are refined until the gradient was below a threshold of $1.0 \cdot 10^{-3}$ a.u.

The recently developed Multipole Derived Charge analysis[183] (see Section 3.1) was used to assign fractional charges and spin densities to the atoms. This analysis uses the atomic multipoles that are obtained by applying an atomic multipole expansion of the Coulomb

potential. The obtained (MDC-q) charges reproduce exactly the atomic multipoles up to the quadrupole moment level and therefore reproduce the Coulomb potential very well, especially in the regions where the higher order moments can be safely ignored. In those regions, the Coulomb potential is reproduced exactly by the MDC-q charges. For systems in a non-singlet ground state (as the ones considered here), the charge density can be obtained for both spins separately. Resulting from these densities are two sets of atomic multipoles (one for spin □, one for spin □), from which two sets of atomic spin charges are obtained. For each atom, the sum of the two spin charges gives the fractional atomic charge, while the difference provides the spin density.

Results and discussion

Complexation of the substrate

The first problem that needs to be solved in order to try to reproduce the experimentally determined E·S state (**2**) lies in the correct positioning of the protons belonging to the system. Owing to the fact that the crystallographic structure used as starting model in the DFT calculations does not contain any information on the location and/or presence of hydrogen atoms, their positions have to be guessed. Three different models have been used in the calculations: **2-dep**, **2-Glu73H** and **2-KMPH**. In the first model (**2-dep**), which has a total charge of zero, the substrate is deprotonated with the proton not present any longer in the system (due to exchange with either solvent or the protein environment); in the second model (**2-Glu73H**), which has a total charge of +1.0, the substrate is deprotonated with the proton located on the $O_{\square 2}$ oxygen (i.e. the oxygen atom not bound to the copper) of the Glu73 side chain; in the last model (**2-KMPH**), the substrate is protonated and Glu73 deprotonated. Based on the short distance between the $O_{\square 2}$ atom of Glu73 and the O_3 atom of the substrate, the second model (**2-Glu73H**) seems to be the most probable, while the third (**2-KMPH**) is chemically not very likely owing to the fact that flavonols are known to be inert towards dioxygen in their protonated form[264]; it has been included for completeness.

The calculations show that the third model (**2-KMPH**) indeed does not need further consideration; the geometry optimization of the structure indicates that a protonated flavonol is incompatible with the presence of a glutamate residue. The 3OH flavonol proton slowly shifts from the substrate to the $O_{\square 2}$ atom of Glu73, leading ultimately to the second model (**2-Glu73H**). This result substantiates the idea of Glu73-mediated deprotonation of the substrate.

The geometries of the optimized **2-dep** and **2-Glu73H** active sites are given in Figure 5.2.4. The overall agreement of the calculated metal-ligand distances and angles with the experimentally observed ones is, for both models, fairly good. However, the short distance between the $O_{\square 2}$ atom of Glu73 and the O_3 atom of the substrate (2.43 Å) found experimentally could be reasonably reproduced only in the **2-Glu73H** model (2.61 Å), in which these atoms are hydrogen bonded. In the other model (**2-dep**), this distance is extremely long (3.16 Å), most likely due to electrostatic repulsion between the negatively charged oxygen atoms (q(MDC-q)=−0.43 for substrate oxygen, −0.54 for Glu73(□2) oxygen). The **2-dep** model exhibits also an unrealistically long Cu-N□2(His112) distance (2.37 Å vs. the experimental value if 2.07±0.04 Å), which is properly reproduced in the **2-Glu73H** model (2.06 Å). On the other hand, the experimental Cu-O□1(Glu73) distance (1.97±0.13 Å) is

more adequately reproduced in **2-dep** (2.08 Å) than in **2-Glu73H** (2.30 Å), but in view of the rather large standard deviation of the experimental Cu-Oε1(Glu73) distance this latter long distance is believed to be less an indication of an improper representation than the deviation from the Cu-Nε2(His112) distance.

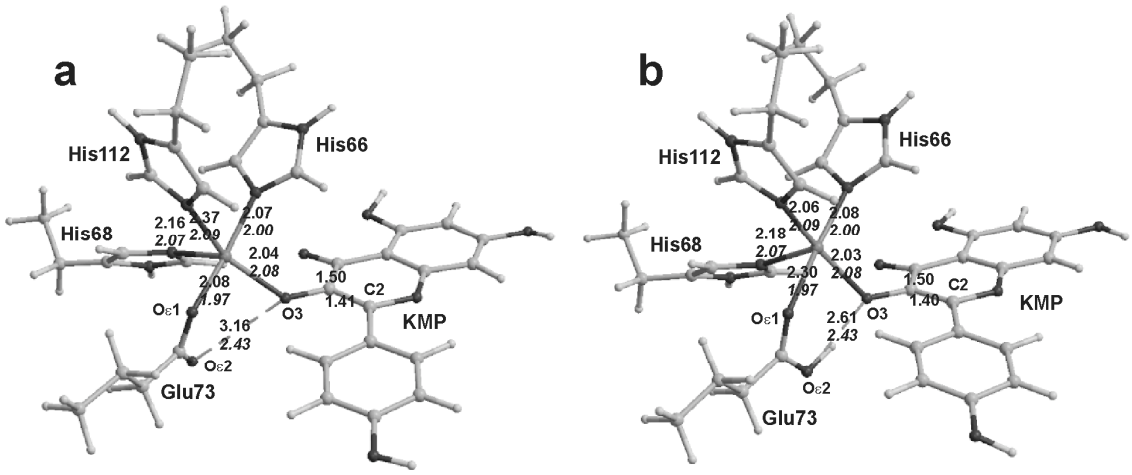

FIGURE 5.2.4. COMPARISON OF COMPUTED AND *EXPERIMENTAL* ACTIVE SITE GEOMETRY OF **2-DEP** (**a**) AND **2-GLU73H** (**b**) MODELS

A direct comparison of the energies of the models favors the **2-Glu73H** model by 290 kcal/mol, but in this comparison a proton (with charge +1) is thought to be transferred infinitely far away. In reality, it will of course have a beneficial interaction with either the solvent or the protein environment, which is ignored in this comparison. A reliable comparison can be made if the "solvation" energies (i.e. the interactions with the protein or solvent environment) are taken into account in the comparison. The "solvation" energies were computed for the **2-dep** and **2-Glu73H** models using the (classical) Direct Reaction Field approach[133-139,141,142,196,197,265-267] (see Section 2.2), where a Boundary Element solution[133,135,137,143] to the Poisson-Boltzmann equation has been used, with a dielectric constant for the protein environment of 20 and using the MDC-q charges for the active site atoms. The proton at infinite distance is assumed to be solvated by water, leading to a solvation energy of –252.39 kcal/mol. The "solvation" energy for the **2-dep** and **2-Glu73H** models are respectively –69.97 and –38.62 kcal/mol, which gives a total stabilization for **2-dep** and $\mathbf{H^+}$ of –322.36 kcal/mol, which is –283.74 more favorable than for the **2-Glu73H** model. Adding the "solvation" and DFT energy differences, the **2-Glu73H** model is more favorable than the **2-dep** model by 6.3 kcal/mol. Therefore, not only on geometric but also on energetic considerations does the **2-Glu73H** model present a better representation for the active site of quercetinase.

An analysis of the spin population in **2-Glu73H** shows that 29 % of the unpaired spin is localized on copper and 28 % on the flavonol ligand (see Table 5.2.1). Significant radical character on the bound substrate molecule is found on the O3 atom (15 %) coordinated to copper and on the C2 atom (13 %). The latter atom is the only one not directly bound to copper having considerable spin density. The partial radical character on C2 supports therefore the existence of a tautomeric complex activated for dioxygen attack (either at C2 or at Cu). An unpaired electron that resides on the O3 atom and to a somewhat lesser extent on the C2 atom

of the substrate is consistent with the results obtained for the oxygenation of potassium flavonolate in DMF, for which a weak EPR signal ascribed to a non-carbon centered radical (g = 2.0038) was observed[263]. Although this latter is believed to proceed with a single electron transfer from the flavonol moiety to dioxygen in order to produce a superoxide anion radical the same **2taut** intermediate is formed in the process.

TABLE 5.2.1. SPIN DENSITIES AND FRACTIONAL CHARGES OF SELECTED ATOMS AND RELATIVE ENERGIES (KCAL/MOL) OF CONFORMATIONS

	2-Glu73H	***3a***	***3b***	***3b2***	***4***	***5***
energy	0.0[a]	−1.20	−2.61	−1.63	+21.15	−87.10[b]
charge						
Cu	+0.53	+0.59	+0.51	+0.52	+0.51	+0.61
C2 (KMP)	+0.20	+0.43	+0.27	+0.37	+0.49	+0.57
C3 (KMP)	+0.22	+0.42	+0.28	+0.29	+0.34	-
O3 (KMP)	−0.58	−0.63	−0.47	−0.45	−0.31	-
C4 (KMP)	+0.29	+0.30	+0.31	+0.31	+0.39	+0.52
O4 (KMP)	−0.43	−0.39	−0.39	−0.39	−0.47	−0.47
Ox1 (O2)	-	−0.22	−0.15	−0.13	−0.24	−0.48
Ox2 (O2)	-	−0.24	−0.14	−0.21	−0.23	−0.52
spin density[c]						
Cu	+0.29	−0.32	−0.27	−0.30	−0.18	−0.35
C2 (KMP)	+0.13	−0.01	+0.03	0.00	−0.03	0.00
C3 (KMP)	+0.02	−0.01	+0.01	0.00	−0.06	-
O3 (KMP)	+0.15	−0.05	+0.01	0.00	−0.01	-
C4 (KMP)	0.00	−0.01	0.00	0.00	+0.01	0.00
O4 (KMP)	+0.03	−0.04	0.00	0.00	−0.21	0.00
Ox1 (O2)	-	−0.04	−0.23	−0.09	−0.01	0.00
Ox2 (O2)	-	−0.05	−0.34	−0.29	−0.06	+0.01

a) energy of isolated dioxygen has been added for relative energy
b) energy of isolated carbonmonoxide has been added for relative energy
c) in **2-Glu73H** the total spin density amounts to one alpha spin in excess, in **3a**/**3b** and further with the presence of triplet dioxygen (two beta spins), the total spin density changes to one beta spin in excess; therefore the sign of the atomic spin densities changes

Dioxygen attack on the C2 flavonol atom

The mechanism of dioxygen attack on an activated ring-position is similar to that proposed for the reaction of the intradiol-type Fe^{3+}-dependent catechol dioxygenases. However, this mechanism has recently been challenged by a DFT study carried out by Funabiki and Yamazaki[268], who reported that they could not obtain a structure of the intermediate arising from dioxygen attack on the catecholate ring of a $[Fe^{3+}(NH_3)_4(catecholate)]^+$ complex. Their explanation was that the catechol ring is positively charged and therefore not prone to dioxygen electrophilic attack; unfortunately, they used Mulliken charges for this explanation, which are known to give the wrong sign for the carbon charges in phenyl rings (see Section 4.3). Moreover, the BLYP[120,227] exchange-correlation potential was used in this

study, which is one of the worst xc-potentials for obtaining geometries, especially when first row transition metals are present (see Section 4.2), and a small basis set was used. The inability to find a structure of the intermediate in their study may be largely influenced by these factors, and therefore does not give any conclusive evidence about the validity of the proposed reaction mechanism.

Even though the C2 atom is positively charged in the **2-Glu73H** model (+0.20), a structure of a dioxygen-substrate adduct **3a** was obtained in this study (see Figure 5.2.5), with an energy that is virtually identical to that of the reactants (see Table 5.2.1). An interesting feature of this complex is that it shows a four-membered 1,2-dioxetane (C3-C2-Ox1-Ox2) structure (Figure 5.2.5). The Ox2 atom of dioxygen is positioned above the C3 atom at a distance of 1.55 Å and not oriented towards the C4 atom as expected in order to form the endoperoxide **4** in the subsequent reaction step. At the time of writing, our various attempts to optimize the structure of peroxide species **3a** in which the Ox2 is near to the C4 atom always failed, leading eventually to the 1,2-dioxetane; a possible peroxide species with Ox2 near C4 is under further investigation.

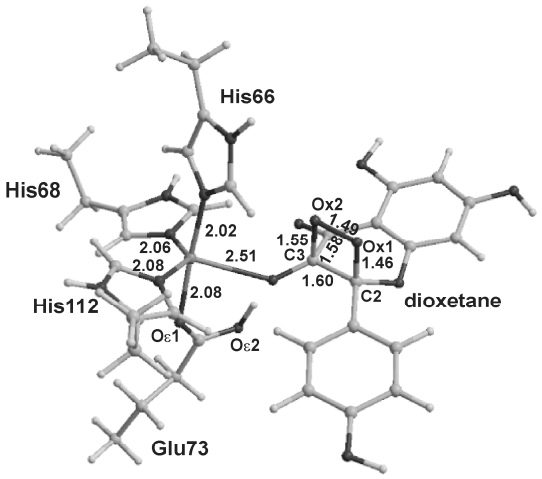

FIGURE 5.2.5. 1,2-DIOXETANE DERIVED FROM DIOXYGEN ATTACK ON KMP

From a geometrical point of view, all protein-metal distances in the 1,2-dioxetane complex are within the range observed experimentally. The Cu-O3 bond is about 0.5 Å longer than found in the experimentally determined E.S complex and 0.2 Å longer than in the computed **2-Glu73H** structure. This longer distance is however still consistent with the dimensions of the active site cavity. Contrary to this, the computed N□2(His68)-Cu-N□2(His112) angle (138°) is outside the normal range observed in the crystal structures (104-115°), and may be an artifact due to the absence of the protein environment in the geometry optimizations.

The existence of a 1,2-dioxetane species as an intermediate in enzymatic reaction should be judged cautiously. Although an early report on the oxygenation of quercetin in aqueous alkaline solution have reported that products consistent with the existence of such an intermediate were obtained[269] this result has later been questioned by Nishinaga and co-workers[270]. Moreover, it is very difficult, as pointed out by the same authors, if not impossible, to reconciliate the existence of a dioxetane intermediate with the experimental

observation from tracer experiment that the substrate's C3 atom is liberated as carbon monoxide, and that none of the atoms of molecular oxygen is incorporated in the leaving CO molecule. The existence of a productive dioxetane intermediate in the enzymatic reactions can, nevertheless, be tested experimentally. These compounds decompose to carbonyl compounds with a very characteristic chemiluminescence[271] which has been observed in the oxygenation of [Cu(phen)(fla)2] (fla = flavonolate, phen = 1,10 phenanthroline) in MeCN[272]. Although no reports which the authors are aware of describe such a phenomenon in quercetinase-mediated dioxygenation of flavonols it is possible that this matter has not been sufficiently investigated. Owing to this result it is clear that some work is necessary to further elucidate this aspect.

Dioxygen attack on copper

Biomimetic studies on a [Cu(II)(fla)(idpa)]ClO4 (fla = flavonolate, idpa = 3,3'-iminobis(N,N-dimethylpropylamine)) complex[273] have indicated the possibility of dioxygen attack on the copper (route **b** of Figure 5.2.3). An analogous proposal has been advanced for the intradiol-type catechol dioxygenases[268], which as already pointed out above, appear to share an activated complex similar to that of quercetinase. The five-coordination of copper in the E S complex indicates that a site for dioxygen binding is, in principle, available at the metal center. The optimized structures arising from such an attack (conformations **3b** and **3b2**) are presented in Figure 5.2.6. From an energetic point of view they are slightly more stable than the reactants, with **3b** and **3b2** being, respectively, 2.6 kcal/mol and 1.6 kcal/mol lower in energy than **2-Glu73H**+dioxygen.

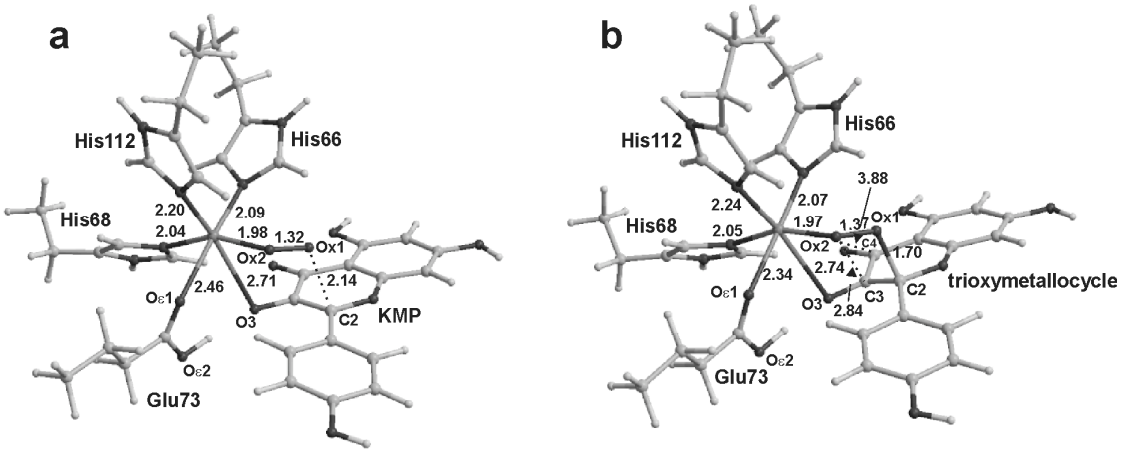

FIGURE 5.2.6. OPTIMIZED STRUCTURES OF CONFORMATIONS **3B** (a) AND **3B2** (b)

The octahedral coordination of structures **3b** and **3b2** features a few long distances. The Cu-Oε1(Glu73) distances (2.46 Å and 2.34 Å in 3b and 3b2, respectively) are slightly longer than observed in the octahedral coordination cage of quercetinase in complex with kojic acid (2.26 Å). The Cu-O3(KMP) and Cu-O3(trioxymetallocycle) distances are considerably longer (~0.7 Å) than in the experimentally determined E S complex. However, this result needs confirmation, for example, by including the protein environment in QM/MM calculations.[a]

[a] Including the protein environment in QM/MM has not been tried, as it would increase the already substantial computational cost even more

In **3b** the Cu-dioxygen distance is 1.97 Å and the Cu-Ox2-Ox1 angle is 119.8°, typical for a 'side-on' O2 binding geometry in which, amongst other interactions, an occupied sp_2 hybrid orbital on dioxygen is coordinated to an empty □-symmetry orbital on the metal. An identical value for the Fe-dioxygen distance is found by Funabiki and Yamazaki[268] in their investigation of the mechanism on the intradiol-type catechol dioxygenase. The Ox1-Ox2 distance of 1.32 Å along with the significant spin density population on dioxygen (23 % on Ox1 and 34 % on Ox2) is consistent with its superoxide anion character. In **3b** the Ox1 atom is found at 2.14 Å from C2. The proper positioning and distribution of charges (q(Ox1) = -0.15; q(C2) = +0.27) supports a nucleophilic attack of the superoxide anion on the flavonol to form the trioxymetallocycle **3b2**. In this compound, the Cu-O3-C3-C2-Ox1-Ox2 atoms form a six-membered ring arranged in a 'chair-conformation'. The Cu-Ox2 distance is virtually identical to that in the **3b** complex but the Ox1-Ox2 distance is elongated, which signifies a transition from a superoxide to a peroxide species. However, the trioxometallocycle still appears to maintain considerable superoxide character owing to the rather short Ox1-Ox2 distance (1.37 Å < 1.45 Å) and the considerable spin density at Ox2 (29 %).

According to the proposal advanced by Barhacs and co-workers[273], the endoperoxide **4** might be generated from the complex **3b2** as a result of an intramolecular nucleophilic attack of the Ox2 atom on the C4 carbon. Although such an attack is not impossible, it appears geometrically not favored in the light of the optimized **3b2** structure. Ox2 and C4 are about 3.9 Å apart and the angle between Ox2-C4 and the direction perpendicular to the carbonyl plane is 55°. An attack of Ox2 on the C3 atom, which would form the previously discussed 1,2-dioxetane, seems more favorable. Ox2 and C3 are about 2.75 Å apart and Ox2 forms an angle of 37° with the accessible p-orbital of C3. From an electrostatic perspective, both C3 and C4 atoms are, as expected, apt to nucleophilic attack by Ox2; C3 and C4 have a charge of +0.29 and +0.31 respectively, whereas Ox2 has a charge of −0.21.

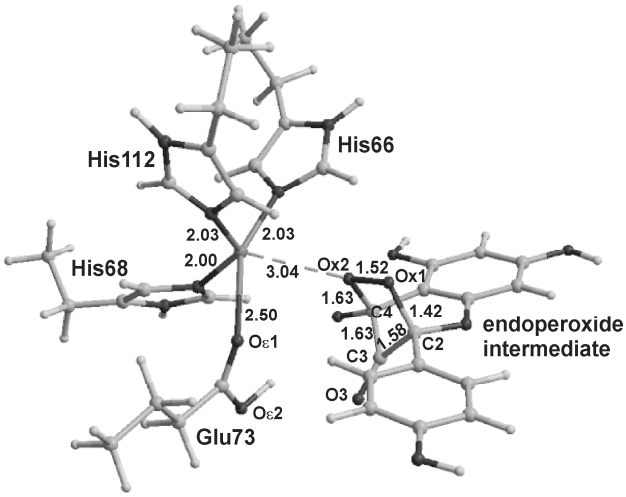

FIGURE 5.2.7. OPTIMIZED STRUCTURE OF ENDOPEROXIDE **4**

*Endoperoxide intermediate **4***

The results discussed above indicate the possibility of the formation of a 1,2-dioxetane species as an intermediate in the quercetinase-catalyzed cleavage of flavonols.

Nevertheless, the five-membered endoperoxide intermediate **4** still represents the best structure in order to rationalize the dioxygenase character of the enzymatic reaction and the liberation of the C3 atom of the substrate as carbon monoxide. The optimization of the structure of the endoperoxide **4** has therefore been performed, with the result presented in Figure 5.2.7. Interestingly, the optimized structure shows that the Ox2-Ox1-C1-C2 dihedral angle has a value of only 9°, which might indicate that the formation of endoperoxide **4** from the 1,2-dioxetane species is not too unfavorable. In the latter structure, the Ox2 and C4 atoms are at 2.4 Å distance. It is therefore possible that a rearrangement of the four-membered ring dioxetane ring driven by nucleophilic attack of Ox2 on the C4 atom produces the five-membered endoperoxide species.

The known instability of such a compound[263] is revealed by its high energy content. It is about 21 kcal/mol less stable than the reactants. Its tendency to easily loose carbonmonoxide with concomitant breakage of the O-O bond is reflected by the very stretched Ox1-Ox2, C2-C3, and C3-C4 bonds. The Ox1-Ox2 distance is 0.07 Å longer than that of a normal peroxide bond. Similarly, the C2-C3 and C3-C4 bonds are considerably longer than in the E S complex (1.58 vs. 1.40 Å, and 1.63 vs. 1.50 Å, respectively). The coordination geometry of this adduct is complex. It can be described as distorted tetrahedral having His66(Nδ2), His66(Nδ2), His68(Nδ2) and Glu73(Oδ1) being the principal ligands. The Oδ1(Glu73) atom is further away from the copper (2.50 Å) than in the other structures. As pointed out earlier, it is difficult to assess whether this longer distance is real or an artifact due to the absence of the protein environment in the calculations. In this structure it seems possible that the absence of the protein environment allows the Glu73 residue to shift in order to maintain the Oδ2(Glu73) atom at hydrogen bond distance to the O3 atom, which moves out of the flavonol plane. Although weak, an interaction might also be present between the copper center and the Ox2 peroxide atom. This appears to be the only direct interaction between the endoperoxide molecule and the catalytic core.

Depside complex ***5***

Air exposure of the anaerobic complex of quercetinase and quercetin produces an EPR spectrum different than that of the native enzyme[260]. This result was interpreted in terms of the formation of an E depside complex. Depside complexation of the quercetinase copper center is not unexpected. The complex [Cu(idpa)(*O*-bs)]ClO4 [idpa = 3,3'-iminobis(N,N-dimethylpropylamine), *O*-bs = O-benzoylsalicylate], which can be obtained from [Cu(idpa)(fla)]ClO4 [fla = flavonolate] with release of CO, has been synthesized and characterized by X-ray crystallography[274]. In this complex the carboxylate group of *O*-bs asymmetrically chelates the copper (Cu-O1 = 1.995(5) Å; Cu-O2 = 2.344(6) Å).

In contrast, the optimized structure of the E depside complex, shown in Figure 5.2.8, reveals that the carboxylate group of the depside product weakly interacts with the copper in a monodentate way (at the long distance of 2.87 Å). This is consistent with the monodentate flavonol binding observed in the anaerobic quercetinase-substrate complexes. From a mechanistic point of view it is interesting to note that in the course of the optimization, the proton originally located on the Oδ2(Glu73) atom drifts to the Ox2 atom of the depside product causing a progressive elongation of the Cu-Ox2 distance. This result supports the idea that in the last step of the catalytic cycle Glu73 protonates the depside product in order to facilitate its release from the active site.

The line-shapes and g-values of the EPR spectrum of the putative E depside complex resemble those reported for Cu^{2+} spectra of model complexes of trigonal bipyramidal geometry[275,276]. The coordination of the copper site in the E depside complex has therefore been suggested to be also trigonal bipyramidal. The optimized structure shows that although some trigonal bipyramidal character is present (His66-Cu-Glu73 is the axial direction), the site has a predominant square pyramidal character (τ index[275] = 0.40). This contradiction may be explained by the fact that this site shows, similar to the structure of the 1,2-dioxetane discussed before, a large His68(Nδ2)-Cu-His112(Nδ2) angle (146°). It exceeds by 40° the average experimental value of quercetinase-substrate complexes, and may be the result of the absence of the protein environment in the calculations. Inclusion of the protein environment in QM/MM calculations[a] might result again in a trigonal bipyramidal site as expected on the basis of the EPR experiment.

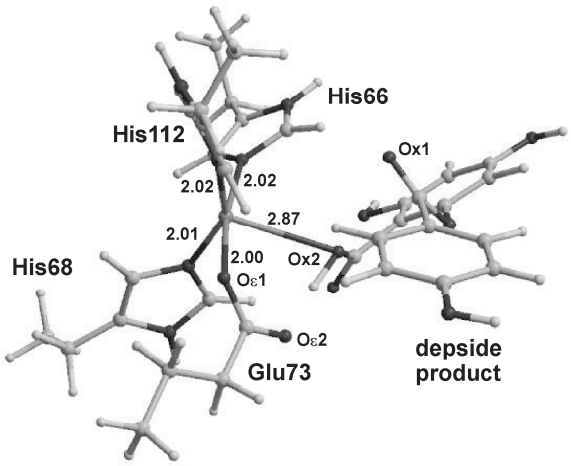

FIGURE 5.2.8. OPTIMIZED STRUCTURE OF E·DEPSIDE COMPLEX **5**

Conclusions

The most generally accepted reaction paths (routes **a** and route **b**) for the quercetinase-mediated dioxygenation of flavonols have been investigated using DFT calculations. The results support the existence of an activated flavonoxy radical-Cu+ complex (**2taut**) that can be attacked by molecular dioxygen. Most likely, the Glu73 copper ligand acts as a base that takes the proton from the incoming flavonol and retains it during catalysis. It is found that the attack of dioxygen on the carbon centered radical of flavonol might lead to a 1,2-dioxetane species. At this moment it is still unclear whether this species really occurs in the catalytic mechanism. Dioxygen attack on the copper center itself appears to be possible also. The trioxymetallocycle **3b2**, which originates from the Cu-superoxide species **3b**, seems to form more easily the dioxetane species than the endoperoxide **4**. This latter intermediate is, however, better suited to explain the chemistry of the enzymatic reaction. As the dioxetane,

[a] Including the protein environment in QM/MM has not been tried, as it would increase the already substantial computational cost even more

3b, and **3b2** species all have virtually the same energy as the reactants, it is not impossible that all these intermediates are unproductive, and that all revert to **2-Glu73H** and free dioxygen, until the proper arrangement for the formation of peroxide **3a** is reached. This elusive peroxide **3a** adduct is under further investigation. However, the five-membered endoperoxide **4** may also be generated by rearrangement of the four-membered dioxetane species. Decomposition of the endoperoxide species **4** is shown to easily form CO with concomitant breakage of the O-O peroxide bond. In the final stage of the reaction Glu73 donates back the proton abstracted in the first step of the mechanism, to facilitate product release.